Absorption Line Survey of H_3^+ toward the Galactic Center Sources I. GCS 3-2 and GC IRS3 †

Miwa Goto [1,2], Benjamin J. McCall [3], Thomas R. Geballe [4], Tomonori Usuda [1], Naoto Kobayashi [1], Hiroshi Terada [1], and Takeshi Oka [5]

[1] *Subaru Telescope, 650, North A'ohoku Place, Hilo, HI 96720, USA*

mgoto@naoj.org,mgoto@duke.ifa.hawaii.edu

[2] *Institute for Astronomy, University of Hawaii, 640, North A'ohoku Place, Hilo, HI 96720, USA*

[3] *Department of Chemistry and Department of Astronomy, University of California, 601 Campbell Hall, Berkeley, CA 94720-3411, USA*

[4] *Gemini Observatory, 670, North A'ohoku Place, Hilo, HI 96720, USA*

[5] *Department of Astronomy and Astrophysics, Department of Chemistry, and Enrico Fermi Institute, University of Chicago, Chicago, IL 60637, USA*

(Received 2002 August 0; accepted 2002 October 0)

Abstract

We present high resolution (R = 20,000) spectroscopy of H_3^+ absorption toward the luminous Galactic center sources GCS 3-2 and GC IRS 3. With the efficient wavelength coverage afforded by Subaru IRCS, six absorption lines of H_3^+ have been detected in each source from 3.5 to 4.0 μm, three of which are new. In particular the 3.543 μm absorption line of the $R(3, 3)^l$ transition arising from the metastable $(J, K) = (3, 3)$ state has been tentatively detected for the first time in the interstellar medium, where previous observations of H_3^+ had been limited to absorption lines from the lowest levels $(J, K) = (1, 0)$ of ortho-H_3^+ and (1, 1) of para-H_3^+.

The H_3^+ absorption toward the Galactic center takes place in dense and diffuse clouds along the line of sight as well as the molecular complex close to the Galactic nucleus. At least four kinematic components are found in the H_3^+ absorption lines. We suggest identifications of the velocity components with those of H I, CO, and H_2CO previously reported from radio and infrared observations. H_3^+ components with velocities that match those of weak and sharp CO and H_2CO lines are attributed to diffuse clouds. Our observation has revealed a striking difference between the absorption profiles of H_3^+ and CO, demonstrating that spectroscopy of H_3^+ provides information complementary to that obtained from CO spectroscopy.

The tentative detection of the $R(3, 3)^l$ line and the non-detection of spectral lines from other $J > 1$ levels provide observational evidence for the metastability of the (3, 3) level, which is theoretically expected. This suggests that other metastable $J = K$

levels with higher J may also be populated.

Key words: ISM: molecules — ISM: lines and bands — ISM: clouds — Galaxy: center

1. Introduction

The crucial role which the H_3^+ molecular ion plays in interstellar chemistry was first addressed by Watson (1973) and Herbst & Klemperer (1973). H_3^+ is produced by cosmic ray ionization of H_2 to H_2^+ followed by the efficient Langevin reaction

$$H_2^+ + H_2 \rightarrow H_3^+ + H. \quad (1)$$

It works as a universal protonator (acid) in the efficient proton hop reaction

$$H_3^+ + X \rightarrow H_2 + XH^+ \quad (2)$$

for most molecules or atoms X (He, Ne, N, and O_2 are a few exceptions). Subsequent general reactions with a molecule Y

$$XH^+ + Y \rightarrow XY^+ + H \quad (3)$$

lead further to chemical networks which produce complex molecules in dense interstellar clouds.

A search for interstellar H_3^+ was initiated by Oka (1981) more than two decades ago, and culminated in the discovery of H_3^+ in the interstellar medium toward AFGL 2136 and W33A, young stellar objects deeply embedded in molecular clouds (Geballe & Oka 1996). Since then the study of interstellar H_3^+ has progressed rapidly by a series of successful observations in dense clouds (McCall et al. 1999) and in diffuse clouds toward the highly reddened star Cygnus OB2 12, the Galactic center, and many other sightlines (McCall et al. 1998b; Geballe et al. 1999; McCall et al. 2002). These observations have not only demonstrated the ubiquity and abundance of this molecular ion which was anticipated in general in molecular hydrogen dominated plasmas (Martin, McDaniel & Meeks 1961), but also revealed an interesting enigma related to the H_3^+ chemistry of the diffuse interstellar medium. While the H_3^+ column densities measured in dense clouds agreed well with those predicted by the H_3^+ production and destruction mechanisms of Herbst & Klemperer (1973) (Geballe & Oka 1996; McCall et al. 1999), those measured in the diffuse interstellar medium have been found to be orders of magnitude higher than estimated using canonical values of plasma chemical constants (McCall et al. 1998a; McCall et al. 1998b; Geballe et al. 1999; McCall et al. 2002). In order to have a better understanding of this problem, we undertook an absorption line survey of this molecular ion toward the Galactic center. This study also provides unique information on the medium toward the Galactic center

† Based on data collected at Subaru Telescope, which is operated by the National Astronomical Observatory of Japan.

because of the special characteristics of H_3^+ as an astrophysical probe.

The absorption line survey is designed to cover the maximum number of H_3^+ absorption lines in clouds with various physical conditions. The Galactic center sources are ideal for this purpose since they suffer heavy visual extinction of $A_V = 25 - 40$ (Cotera et al. 2000), the highest in the Galaxy among those obscured mainly by diffuse clouds. The line of sight to the Galactic center cuts through dense and diffuse clouds in the intervening spiral arms as well as the molecular complex close to the nucleus. Thus, H_3^+ in different physical conditions is efficiently sampled in one observation. The intervening clouds have different radial velocities, and the nature of the clouds have been studied in previous spectroscopic observations using molecular and atomic tracers from near-infrared to radio wavelengths. Two infrared sources, GCS 3-2 in the Quintuplet cluster (Nagata et al. 1990; Okuda et al. 1990) and GC IRS 3 (Becklin & Neugebauer 1975; Becklin et al. 1978) near Sgr A* have been selected since both appear to have intrinsically featureless spectra due to dust emission and are sufficiently luminous to provide good continuum fluxes for L-band absorption spectroscopy.

Wide wavelength coverage is essential for a line survey. Observation of interstellar H_3^+ has so far been almost entirely limited to the three absorption lines, $R(1, 0)$, $R(1, 1)^l$, and $R(1, 1)^u$, all arising from the lowest $J = 1$ rotational levels, i.e. $(J, K) = (1, 0)$ of ortho-H_3^+ and (1, 1) of para-H_3^+ (note that the $J = 0$ level is forbidden by the Pauli principle; McCall 2001). This is because high spectral resolution and wide wavelength coverage are often incompatible. This limitation has now been overcome by a new generation of cross dispersed infrared spectrographs, such as IRCS on the Subaru Telescope. We can now simultaneously observe at high spectral resolution not only most of the transitions starting from the $J = 1$ levels, including $Q(1, 0)$ and $Q(1, 1)$, but also other transitions starting from higher J levels. This wide coverage has led us to a tentative detection of the $R(3, 3)^l$ line starting from the metastable $(J, K) = (3, 3)$ level.

2. Observation

These spectroscopic observations were made on UT 2001 June 16 using the Infrared Camera and Spectrograph (IRCS; Tokunaga et al. 1998; Kobayashi et al. 2000) with the 8.2 m Subaru Telescope on Mauna Kea. Subaru IRCS is equipped with an echelle and a cross-dispersing grating to offer high resolution spectroscopy without sacrificing wavelength coverage. Figure 1 shows the wavelength coverage of the IRCS echelle mode in the 3 μm region. The entire L-band (2.84–4.18 μm) can be covered with six standard settings, with 70% coverage in three settings. Thus, Subaru IRCS is a good match for a survey of lines scattered in a single band. The grating setting can be modified continuously for the best coverage of target lines in order to maximize observing efficiency.

In the current experiment we employed two grating settings optimized for coverage of the $\nu_2 \leftarrow 0$ H_3^+ lines in the 3 μm region illustrated in Figure 1. At the time of the observations, there was high dark current in the upper two quadrants of the 1k $\times$ 1k InSb detector array, so we covered the relevant wavelength ranges using only the lower half of the array. The wavelengths of major H_3^+ lines as measured in the laboratory (Oka 1980; Oka 1981; McKellar & Watson 1998; Lindsay & McCall 2001) and the coverages are listed in Table 1. A $0.''15 \times 4.''5$ slit was used to achieve R = 20,000 spectral resolution. The spectra were recorded by nodding the telescope between two points separated by $2.''2$ along the slit to subtract sky emission and dark current. Spectroscopic standard stars were observed through airmasses similar to those of the objects in order to cancel out the atmospheric transmission efficiency. The details of the observations are summarized in Table 2. The seeing was not better than $0.''7$ at L', and varied during the observing period. Spectroscopic flat frames were obtained at the end of the night with a halogen lamp in the telescope calibration unit installed in front of the instrument window.

3. Data Reduction

The observed spectrogram images were stacked and averaged without pixel registration since both the accumulation of the instrument flexure and the telescope tracking error during automated guiding is negligible over the typical tracking period. The average frame was flat-fielded with the dark-subtracted halogen lamp frame. Bad pixel masks were created by collecting pixels with low, high, and varying responses, and high dark current, based on the statistics of the halogen lamp and the dark current frames. Those outliner pixels were filtered out before spectral extraction.

One dimensional spectra were obtained using the IRAF[1] aperture extraction package. Spectroscopy in the 3 μm region suffers severely from interference by the absorption lines of molecules in Earth's atmosphere. Poor cancellation of the atmospheric lines during ratioing by standard stars is often the primary source of systematic errors, which easily overwhelm statistical noise. We carefully examined the locations of the H_3^+ lines listed in Table 1 using a custom written IDL code. The code handles (1) linear registration of the wavelength offset between the object and the spectroscopic standard, (2) rescaling the normalized standard star spectrum according to Beer's law to minimize the airmass mismatch that sometimes exceeded 10% in our observation, and (3) correction of the spectral resolution by deconvolving the spectra. Wavelength calibration was performed by maximizing the cross correlation between the object spectrum and the model atmospheric spectrum calculated by ATRAN code (Lord 1992).

[1] IRAF is distributed by the National Optical Astronomy Observatories, which are operated by the Association of Universities for Research in Astronomy, Inc., under cooperative agreement with the National Science Foundation.

4. Results

The result of the line survey is shown in Figure 2 and Figure 3 for the positive and negative detections, respectively. The model atmospheric transmission curves convolved to the same spectral resolution are shown in order to discriminate between real spectral features and residual features of the strong telluric absorption lines. All the absorption lines in our coverage starting from the lowest $J = 1$ levels of ortho- and para-H_3^+ [$R(1, 0)$, $Q(1, 0)$, $R(1, 1)^l$, $R(1, 1)^u$, and $Q(1, 1)$] are successfully detected, while those from $J > 1$ levels are all negative except $R(3, 3)^l$.

The H_3^+ absorption lines from the $J = 1$ levels show several discrete kinematic components. The absorption profiles are deconvolved into Gaussian components centered at LSR velocities of -110 – -140 km s^{-1}, -50 – -60 km s^{-1}, and 0 km s^{-1} (Fig. 4). The deconvolution parameters are summarized in Table 3. GC IRS 3 shows wide absorption at -20 km s^{-1} and a wing at +50 km s^{-1} on a broad pedestal absorption. A weak absorption is seen at -170 km s^{-1} in GCS 3-2. Note that the velocity components are less distinguishable at 3.668 μm, previously observed toward the Galactic center (Geballe et al. 1999). This is because the absorption feature consists of a close doublet of $R(1, 0)$ and $R(1, 1)^u$ transitions with a separation of $\Delta v =$ 35 km s^{-1}.

The column density of H_3^+ has been derived from the observed equivalent width W_λ using the equation $W_\lambda = (8\pi^3\lambda/3hc)N|\mu|^2$, where N is the column density of H_3^+ in the lower state of the transition. The values of $|\mu|^2$ listed in Table 1 have been used. The velocity integrated column densities of individual transitions are summarized in Table 1. For the absorption lines with quality to allow Gaussian deconvolution the column density of each velocity component is calculated and shown in Table 3.

5. Discussion

5.1. *Location of H_3^+ Absorbing Clouds*

We discuss below the possible identifications of the absorbing clouds, referring to previous observations at radio and infrared wavelengths shown in Figure 5. We will base the following velocity discussion on GC IRS 3 spectral lines unless otherwise stated, since the line profiles are sharper than those of GCS 3-2.

5.1.1. *-140 km s^{-1} to -110 km Component*

The -140 km s^{-1} component is attributed to clouds in the "expanding molecular ring" (Kaifu, Kato, & Iguchi 1972; Scoville 1972). The "expanding molecular ring" is a chain of molecular clouds orbiting around the nucleus at 200 pc from the Galactic center and gradually receding from it. The -140 km s^{-1} component of GC IRS 3 appears at -110 km s^{-1} in GCS 3-2, which is reasonable because the "expanding molecular ring" appears with a less negative velocity at positive Galactic longitude. The additional possible peak at -170 km s^{-1} seen towards GCS 3-2 could be the high velocity component discussed by Güsten & Downes (1981), Liszt & Burton (1993), and Yusef-Zadeh, Lasenby, & Marshall (1993).

5.1.2. -60 km s^{-1} Component

A clear match of peak velocities at -60 km s^{-1} is noted between the H_3^+ lines and the H_2CO line observed in absorption toward Sgr A (Snyder et al. 1969; Güsten & Downes 1981), and the HI absorption line (Liszt, Burton, & van der Hulst 1985). The cloud velocity is consistent with the radial velocity of the "3 kpc arm". The "nuclear disk" rotating at 300 pc from the Galactic center (Sanders & Wrixon 1973) also shows a similar velocity at the longitude of GC IRS 3 (Whiteoak & Gardner 1979). However, we infer that the contribution of the "3 kpc arm" clouds is dominant since the component is also seen in GCS 3-2 at the same velocity. This interpretation is also supported by the absence of a positive velocity component which is expected from the "nuclear disk" for the positive Galactic longitude of GCS 3-2.

5.1.3. 0 km^{-1} Component

The 0 km s^{-1} component is also apparent in H_2CO and HI absorption spectra of Sgr A in Figure 5. The 0 km s^{-1} absorbers are usually attributed to the "local clouds" within a few kpc of the solar neighborhood, which is most evident in the HI absorption at 21 cm (e.g., Garwood & Dickey 1989). There should also be a contribution from the low velocity dense clouds close to Sgr A. Some of them are reported to be within about 50 pc of Sgr A by Whiteoak & Gardner (1978).

5.1.4. +50 km^{-1} Wing

A candidate for the H_3^+ absorption wing at +50 km s^{-1} is the "+50 km s^{-1} clouds," a complex of giant molecular clouds within about 10 pc of the Galactic nucleus (Güsten, Walmsley, & Pauls 1981; Güsten & Henkel 1983). In the model of the large scale structures in the central 10 pc of our Galaxy constructed with recent high spatial resolution radio observations (Coil & Ho 2000; Wright et al. 2001), the Sgr A East non-thermal radio source is impacting the "+50 km s^{-1} clouds" at the far side of the Galactic center. If the H_3^+ absorption wing at +50 km s^{-1} is associated with these giant molecular clouds, it places GC IRS 3 beyond Sgr A, which then jeopardizes the membership of GC IRS 3 in the central star cluster. Instead, to account for the absorption feature of CO in the near-infrared at 4.7 μm, Geballe, Baas, & Wade (1989) proposed that the particular cloud occulting GC IRS 3 could be a part of the "circumnuclear disk" delineated by Güsten et al. (1987) in their HCN map. The "circumnuclear disk" is a compact ($\sim$ 3 pc) clumpy torus, a reservoir supposedly feeding mass to the dynamical center of our Galaxy, Sgr A*. The +50 km s^{-1} component is barely seen in GCS 3-2, which suggests that the absorber of GC IRS 3 is a compact local structure at Sgr A, and thus argues in favor of the "circumnuclear disk" origin.

5.2. *Special Characteristic of H_3^+ Number Density*

Lines of sight toward the Galactic center sample both dense and diffuse clouds along the long pathlength. About 30% of the visual extinction toward the Galactic center is believed to arise in dense clouds, and the rest in diffuse clouds (e.g. Whittet et al. 1997). For instance, the diffuse and dense cloud extinctions to GC IRS 3 estimated from the optical depths of hydrocarbon and water ice in the 3 μm region (Chiar et al. 2002) are $A_V = 36$ and $A_V = 11$, respectively.

The optical depth of H_3^+, however, does not scale with the visible extinction. In contrast to most other molecules, the number density of H_3^+ is constant and independent of the density of the cloud as long as the number density of H_2 relative to that of the destroyer X of H_3^+, $n(H_2)/n(X)$, is constant (Fig. 6). A simple analysis using steady state chemical kinetics yields the H_3^+ number density of $n(H_3^+) = (\zeta/k_{CO})[n(H_2)/n(CO)]$ for a typical dense cloud where carbon atoms are mostly in the form of CO, and $n(H_3^+) = (\zeta/k_e)[n(H_2)/n(e)]$ for a typical diffuse cloud where carbon atoms are in the form of C^+ (ζ is the cosmic ray ionization rate, and k_{CO} and k_e are the rate constants of the ion-neutral reaction between H_3^+ and CO and of dissociative electron recombination of H_3^+, respectively; McCall et al. 1998a; McCall et al. 1998b). If typical values of $\zeta \sim 3 \times 10^{-17}$ s^{-1}, $k_{CO} \sim 2 \times 10^{-9}$ cm^3 s^{-1}, $k_e \sim 5 \times 10^{-7}$ cm^3 s^{-1} are used, and $[n(H_2)/n(CO)]$ and $[n(H_2)/n(e)]$ are both assumed to be 7×10^3, we obtain $n(H_3^+)$ $\sim 1 \times 10^{-4}$ cm^{-3} in dense clouds and $\sim 4 \times 10^{-7}$ cm^{-3} in diffuse clouds. These constancies of the number density make H_3^+ nearly a direct indicator of the dimension of the absorbing clouds. In other words, regardless of how high or low the cloud density is, the H_3^+ column density is simply proportional to the physical dimension of the cloud along the line of sight. This simple analysis explains the observed H_3^+ column densities in dense clouds well (McCall et al. 1999).

However, a problem appears when this model is applied to diffuse clouds because of uncertainties of the constants used in the calculation. Since the observed H_3^+ column densities in dense and diffuse clouds are comparable, the large factor of 250 difference in $n(H_3^+)$ leads to the same large difference in cloud dimension, which is difficult to accept (McCall et al. 1998a; McCall et al. 1998b; Geballe et al. 1999; McCall et al. 2002). Currently at least one of the three assumed values, ζ, k_e, and $n(e)$ is under suspicion. For instance, measurements of k_e vary more than one order depending on the experimental techniques (e.g. Larsson 2000). Some laboratories have presented smaller values of k_e using storage rings that may reconcile the expected $n(H_3^+)$ to the observation in diffuse clouds (Sundström et al. 1995; Jensen et al. 2001). It is likely that the estimate of $n(H_3^+)$ in diffuse clouds will be increased by one order of magnitude or so when this is corrected; $n(H_3^+)$ will then give a reasonable cloud dimension.

5.3. *H_3^+ in Diffuse Clouds*

The sharp and weak H_2CO lines toward Sgr A at -140 km s^{-1}, -60 km s^{-1} and 0 km s^{-1}, and the weakness of CO absorption at these velocities in GC IRS 3 indicate that the clouds responsible for those absorptions are diffuse. Geballe, Baas, & Wade (1989) estimated the CO column density in the cloud at -60 km s^{-1} velocity to be 1×10^{17} cm^{-2} with cloud temperature 17 K. If we use $[H_2]/[CO] = 7 \times 10^3$, we obtain $N(H_2) = 7 \times 10^{20}$ cm^{-2}, though this value might be better taken as a lower limit because of the possible saturation in the CO fundamental lines. Such a low hydrogen column density is consistent with diffuse clouds.

The observed H_3^+ column density in each of these velocity components of GC IRS 3 is in the range $N(H_3^+) = (2.4–5.6) \times 10^{14}$ cm^{-2}. If the H_3^+ number density in diffuse clouds given above (4×10^{-7} cm^{-3}) is assumed, we obtain the unreasonably high cloud dimensions of 200 to 500 pc. The enigma of H_3^+ chemistry in the diffuse interstellar medium needs to be solved before we discuss the cloud dimension further.

The large pedestal component of GC IRS 3 is also interpreted to be due to diffuse clouds, because of the absence of strong CO or H_2CO absorption. The clarification of the nature of this cloud is an interesting future problem. There exists a possibility that the decomposition of the observed features into velocity components is not unique in view of the significant noise in the spectrum and the limited spectral resolution.

5.4. H_3^+ in Dense Clouds

The strong and saturated CO absorption toward GC IRS 3 and H_2CO for Sgr A at the velocity of +50 km s^{-1} wing clearly represent dense clouds (Fig. 5). It is remarkable that the H_3^+ absorption lines starting from the $J = 1$ levels are weak at this velocity (Fig. 2). This must be due to a small pathlength of a very dense cloud in front of the infrared source. From the equivalent width of the $R(1, 1)^l$ line integrated over +20 to +60 km $^{-1}$, $N(H_3^+)_{J=1} = 2.4 \times 10^{14}$ cm^{-1} is obtained; this corresponds to a dense cloud pathlength of 1.1 pc if $n(H_3^+) \sim 1 \times 10^{-4}$ cm^{-3} estimated in Section 5.2 is assumed. The concentration of the H_3^+ in (3, 3) level at the velocity would increase the total column density and the cloud dimension, however, we leave the population uncounted because we do not have enough knowledge about either the nature of the cloud that holds H_3^+ in the (3, 3) level or the mechanism that populates the metastable states, which we discuss separately in the next subsection.

The cloud dimension of +50 km s^{-1} wing might not be incompatible with the "+50 km s^{-1} clouds" interpretation in terms of the physical parameters presented by Güsten & Henkel (1983). They estimate the hydrogen column density of M-0.02-0.07, the closest "+50 km s^{-1} cloud" to GC IRS 3, to be $N(H_2) = 7 \times 10^{24}$ cm^{-2} which gives $n(H_2) = 2 \times 10^6$ cm^{-3} if the cloud dimension of 1 pc is assumed. The angular diameter of M-0.02-0.07 is $2'$ in Güsten & Henkel (1983), which is 5 pc at the assumed 8 kpc distance. The apparent smaller pathlength measured by H_3^+ could be reconciled if the line of sight toward GC IRS 3 is off-centered from the cloud core.

On the other hand the physical model of the "circumnuclear disk" proposed by Marshall, Lasenby, & Harris (1995) gives the radial thickness of the annular disk to be 0.5 pc with hydrogen density $n(H_2) \simeq 10^6$ cm^{-3}. The factor 2–3 difference could be filled by the geometry of GC IRS 3 and the disk.

5.5. *H_3^+ in Metastable State*

The tentative detection of the $R(3, 3)^l$ transition at 3.534 μm for the first time in interstellar space would be a breakthrough if confirmed by more observations; it introduces a new dimension in the studies of interstellar H_3^+. The detection of $R(3, 3)^l$ and non-detection of other transitions starting from $J > 1$ levels such as $R(2, 1)^u$, $R(2, 2)^l$, $Q(2, 1)^l$, $Q(3, 0)$ etc. is reasonable since only the (3, 3) rotational level is metastable; spontaneous emission from this level to lower levels is forbidden by the ortho-para selection rule and the absence of the (2, 0) rotational level by the Pauli principle, as shown in Figure 7 (Pan & Oka 1986). On the other hand, H_3^+ in the (2, 1), (2, 2), (3, 0), (3, 1), and (3, 2) levels decays to lower levels with lifetimes of 20.4 days, 27.2 days, 3.8 hours, 7.9 hours and 15.8 hours, respectively (Neale, Miller, & Tennyson 1996) through the centrifugal distortion induced rotational transitions initially proposed for NH_3 (Oka et al. 1971). Since detailed *ab initio* quantum chemical calculations of H_3^+ have been extensively carried out, these lifetimes are accurate and reliable. All ortho-H_3^+ which are chemically produced or collisionally pumped into the (4, 3), (3, 0), and (3, 3) levels accumulate in the (3, 3) level until it is collisionally deexcited to lower levels. Similarly ortho-H_3^+ produced in (5, 3), (5, 0), (6, 6), (6, 3), (7, 6), (7, 3), (7, 0) etc. accumulate in the (6, 6) metastable level. Metastable levels are also expected for para-H_3^+, for which (4, 4) and (5, 5) may be excessively populated. H_3^+ in the (4, 4) level can spontaneously decay to the (3, 1) level but its lifetime is long (11 years).

H_3^+ in metastable levels relaxes to lower levels by collisions with H_2. Unlike NH_3 in which ortho $\leftrightarrow$ para transitions are forbidden for collision induced transitions (Cheung et al. 1969), H_3^+ may relax to lower levels of different spin modification. This is because a collision of H_3^+ with H_2 is a chemical reaction and the scrambling of protons may change ortho-H_3^+ into para-H_3^+ or vice versa, although some selection rules for nuclear spin still remain (Uy, Cordonnier, & Oka 1997; Cordonnier et al. 2000).

There are two ways that the (3, 3) level could be populated significantly compared with the lowest $J = 1$ levels. First, it may be simply because of high temperature. The (3, 3) level is higher than the lowest (1, 1) level by 251.23 cm^{-1} (361 K) and the populations of the two levels become equal at $T = 234$ K. Populations in excited non-metastable levels may be still low even at high temperature because of fast spontaneous emission, if the cloud density is lower than the critical densities of the levels. The critical densities are on the order of 10^4 cm^{-3} for (2, 1) and (2, 2) and 10^6 cm^{-3} for (3, 0), (3, 1) and (3, 2). Thus our observation of the $R(3, 3)^l$ transition and non-detection of other transitions starting from $J > 1$ levels indicate low density. When the metastable state is positively confirmed to be thermally populated, then the $R(3, 3)^l$ transition and other absorption lines from metastable levels make an excellent probe to efficiently isolate the warm interstellar gas. These absorption lines are unique in that they are sensitive exclusively to the high temperature clouds ($T \sim 200$ K) along the line of sight with minimum contamination by other cold clouds.

Second, the excess population at (3, 3) could occur at low temperature with a subtle balance of the rate of collisional deexcitation and destruction of H_3^+. If the former rate, $k_{\rm H} n(H_3^+) n(H_2)$, is much faster than the latter, $k_{\rm X} n(H_3^+) n({\rm X})$, H_3^+ at low temperature will all relax to the lowest $J = 1$ levels during its lifetime. The excess population in (3, 3) could occur only when those rates are comparable, that is, $k_{\rm H} n(H_2) \sim k_{\rm X} n(H_{\rm X})$. This cannot happen in dense clouds where CO is the main destroyer of H_3^+ since $k_{\rm H} \sim k_{\rm CO}$ and $n(H_2) \gg n({\rm CO})$. For diffuse clouds this may be possible if $n(H_2)/n(e)$ is not much larger than $k_e/k_{\rm H} \sim 250$. For this to happen a high electron density and high k_e is preferred. It is interesting to note that the latter requirement is opposite to what is needed to reconcile the enigma of the observed high column densities of H_3^+ in the diffuse interstellar medium.

Although our detections of the $R(3,\ 3)^l$ line look fairly convincing for both GC IRS 3 and GCS 3-2, we note both lines are broad and without sharp velocity component. In addition, the spectral line toward GC IRS 3 is enigmatic in that the five spectral lines starting from the $J = 1$ level are not strongly observed at the velocity of the $R(3,\ 3)^l$ line. A simple model calculation shows that it is hard to populate the (3, 3) level alone without populating the (1, 0) and (1, 1) level. It is intriguing that the line profile of $R(3,\ 3)^l$ is similar to those of the strongly saturated CO line both in its wavelength and widths (Fig. 5). Such CO lines indicate dense clouds where H_3^+ will be collisionally cooled rapidly to lower levels. We may be sampling low density warm gas with long pathlength surrounding such dense cloud.

The high population in the (3, 3) level makes the problem of the unexpectedly high abundance in diffuse clouds even harder to reconcile, since other metastable states may also be significantly populated. The need of a high value of k_e for the second mechanism to populate (3, 3) is also an interesting twist related to the enigma. We will attempt to observe more objects and more spectral lines starting from metastable levels, and to carry out detailed analysis of this problem.

6. Summary

We have presented an absorption line survey of H_3^+ toward two Galactic center sources: GCS 3-2 in the Quintuplet cluster and GC IRS 3 near Sgr A*. Six H_3^+ lines were detected for each source, of which three are newly detected. In particular the absorption of H_3^+ originating from the $(J,\ K) = (3,\ 3)$ metastable state was tentatively detected for the first time in interstellar space. The observed H_3^+ absorption lines show intriguing line profiles, indicating at least four velocity components of clouds along the line of sight. The velocities match well with those of HI, CO, and H_2CO reported earlier in the radio and infrared. The H_3^+ velocity components at 0, -60, and -110 – -140 km s^{-1}, which match well with those of sharp and weak CO as well as with H_2CO, are inferred to be in the diffuse interstellar medium in intervening spiral arms, while the +50 km s^{-1} component in GC IRS 3 should be associated with the local structure of the Galactic nucleus. Surprisingly, not much H_3^+ is found at +50 km s^{-1} where very strong and saturated CO absorption is observed in GC IRS 3. This shows the stark contrast between CO and H_3^+ as astrophysical probes; the number density of CO is proportional to the cloud density while that of H_3^+ is independent of the cloud density.

The tentative detection of the $R(3,\ 3)^l$ line provides observational evidence for the metastability of the (3, 3) level, which had been theoretically expected. It suggests that other metastable $J = K$ levels may also be populated. While the observed H_3^+ spectra reveal the great richness of the sight lines toward Galactic center, there are many loose ends in our interpretation of the spectra. Further studies on the H_3^+ spectrum as well as on CO and H_2 spectroscopy toward the Galactic center will be attempted to further clarify the situation.

We acknowledge all the staff and crew of the Subaru Telescope and NAOJ for their valuable assistance obtaining this data and their continuous support for the construction of IRCS. We wish to appreciate the anonymous referee for useful comments on the manuscript. Special thanks goes to K. S. Usuda for many inspiring discussions. B. J. M. is supported by the Miller Institute for Basic Research in Science. T. O. is supported by NSF grant PHY 00-99442. T. R. G.'s research is supported by the Gemini Observatory, which is operated by the Association of Universities for Research in Astronomy, Inc., on behalf of the international Gemini partnership of Argentina, Australia, Brazil, Canada, Chile, the United Kingdom and the United States of America. M. G. is supported by a Japan Society for the Promotion of Science fellowship. Last but not least we wish to express our deep appreciation for those of Hawaiian ancestry on whose sacred mountain we are privileged to be guests.

References

Becklin, E. E., & Neugebauer, G. 1975, ApJ, 200, L71

Becklin, E. E., Matthews, K., Neugebauer, G., & Willner, S. P. 1978, ApJ, 219, 121

Blum, R. D., Sellgren, K., & DePoy, D. L. 1996, ApJ, 470, 864

Cheung, A. C., Rank, D. M., Townes, C. H., Knowles, S. H., & Sullivan, W. T., III 1969, ApJ, 157L, 13

Chiar, J. E., Adamson, A. J., Pendleton, Y. J., Whittet, D. C. B., Caldwell, D. A., & Gibb, E. L. 2002, ApJ, 570, 198

Coil, A. L., & Ho, P. T. P. 2000, ApJ, 533, 245

Cordonnier, M., Uy, D., Dickson, R. M., Kerr, K. E., Zhang, Y., & Oka, T. 2000, J. Chem. Phys. 113, 3181

Cotera, A. S., Simpson, J. P., Erickson, E. F., Colgan, S. W. J., Burton, M. G., & Allen, D. A. 2000, ApJ, 129, 123

Garwood, R. W., & Dickey, J. M. 1989, ApJ, 338, 841

Geballe, T. R., Baas, F., & Wade, R. 1989, A&A, 208, 255

Geballe, T. R., & Oka, T. 1996, Nature, 384, 334

Geballe, T. R., McCall, B. J., Hinkle, K. H., & Oka, T. 1999, ApJ, 510, 251

Güsten, R., & Downes, D. 1981, A&A, 99, 27

Güsten, R., Walmsley, C. M., & Pauls, T. 1981, A&A, 103, 197

Güsten, R., & Henkel, C. 1983, A&A, 125, 136

Güsten, R., Genzel, R., Wright, M. C. H., Jaffe, D. T., Stutzki, J. & Harris, A. I. 1987, ApJ, 318, 124

Herbst, E., & Klemperer, W. 1973, ApJ, 185, 505

Jensen, M. J., Pedersen, H. B., Safvan, C. P., Seiersen, K., Urbain, X., & Andersen, L. H. 2001, Phys. Rev. A, 63, 052701-1

Kaifu, N., Kato, T., & Iguchi, I. 1972, Nature, 238, 105

Kobayashi, N., Tokunaga, A. T., Terada, H., Goto, M., Weber, M., Potter, R., Onaka, P. M., Ching, G., Young, T. T., Fletcher, K., Neil, D., Robertson, L., Cook, D., Imanishi, M., & Warren, D. W. 2000, Proc. SPIE, 4008, 1056

Larson, M. 2000, Phil. Trans. R. Soc. Lond. A. 2000, 358, 2433

Lindsay, C. M., & McCall, B. J. 2001, J. Mol. Spectrosc., 210, 60

Liszt, H. S., Burton, W. B., & van der Hulst, J. M. 1985, A&A, 142, 237

Liszt, H. S. & Burton, W. B. 1993, ApJL, 407, L25

Lord, S. D. 1992 NASA Technical Memoir 103957

Marshall, J., Lasenby, A. N., & Harris, A. I. 1995, MNRAS, 277, 594

Martin, D. W., McDaniel, E. W., & Meeks, M. L. 1961, ApJ, 134, 1012

McCall, B. J., Geballe, T. R., Hinkle, K. H., & Oka, T. 1998, Science, 279, 1910

McCall, B. J., Hinkle, K. H., Geballe, T. R., & Oka, T. 1998, Faraday Discuss., 109, 267

McCall, B. J., Geballe, T. R., Hinkle, K. H., & Oka, T. 1999, ApJ, 522, 338

McCall, B. J., 2001, Ph.D. Thesis, University of Chicago

McCall, B. J., Hinkle, K. H., Geballe, T. R., Moriarty-Schieven, G. H., Evans II, N. J., Kawaguchi, K., Takano, S., Smith, V. V., & Oka, T. 2002, ApJ, 567, 391

McKellar, A. R. W., & Watson, J. K. G. 1998, J. Mol. Spectrosc., 191,215

Nagata, T., Woodward, C. E., Shure, M., Pipher, J. L., & Okuda, H. 1990, ApJ, 351, 83

Neale, L, Miller, S., & Tennyson, J. 1996, ApJ, 464, 516

Oka, T., Shimizu, F. O., Shimizu, T., & Watson, J. K. G. 1971, ApJ, 165, L15

Oka, T. 1980, Phys. Rev. Lett., 45, 531

Oka, T. 1981, Phil. Trans. R. Soc. Lond. A, 303, 543

Okuda, H., Shibai, H., Nakagawa, T., Matsuura, H., Kobayashi, Y., Kaifu, N., Nagata, T., Gatley, I., & Geballe, T. R. 1990, ApJ, 351, 89

Pan, F.-S., & Oka, T. 1986, ApJ, 305, 518

Sanders, R. H., & Wrixon, G. T. 1973, A&A, 26, 365

Sundström, G., Mowat, J. R., Danared, H., Datz, S., Brostöm, Filevish, A., Källberg, Mannervik, S., Rensfelt, K. G., Sigray, P., af Ugglas, M., & Larsson, M. 1994, Science, 263, 785

Scoville, N. Z. 1972, ApJ, 175, L127

Snyder, L. E., Buhl, D., Zuckerman, B., & Palmer, P. 1969, Phys. Rev. Lett., 22, 679

Tokunaga, A. T., Kobayashi, N., Bell, J., Ching, G., K., Hodapp, K-.W., Hora, J. L., Neill, D., Onaka, P. M., Rayner, J. T., Robertson, L., Warren, D. W., Weber, M., & Young, T. T. 1998, Proc. SPIE, 3354, 512

Uy, D., Cordonnier, M., & Oka, T. 1997, Phys. Rev. Lett. 78, 3844

Watson, W. D. 1973, ApJ, 182, L73

Whiteoak, J. B., & Gardner, F. F. 1978, Proc. A. S. A. 3, 266

Whiteoak, J. B., & Gardner, F. F. 1979, MNRAS, 188, 445

Whittet, D. C. B., Boogert, A. C. A., Gerakines, P. A., Schutte, W., Tielens, A. G. G. M., de Graauw, Th., Prusti, T., van Dishoeck, E. F., Wesselius, P. R., & Wright, C. M. 1997, ApJ, 490, 729

Wright, M. C. H., Coil, A. L., McGary, R. S., Ho, P. T. P, & Harris, A. I. 2001, ApJ, 551, 254

Yusef-Zadeh, F., Lasenby, A., & Marshall, J. 1993, ApJL, 410, L27

Table 1. Major absorption lines of H_3^+ $\nu_2 \leftarrow 0$ targeted in the survey. The laboratory data are from McKellar & Watson (1998) and Lindsay & McCall (2001). The velocity integrated equivalent widths and the column densities are summarized for detected lines.

Transition	$\lambda_{\rm Lab}$ [μm][a]	$\lvert\mu\rvert^2$ [D^2][b]	Coverage	W_λ [$10^{-5}\mu$m]		$N_{\rm level}$ [10^{15} cm^{-2}]	
				GCS 3-2	GC IRS3	GCS 3-2	GC IRS3
$R(3,3)^u$ ...	3.426974	0.0071	-				
$R(3,3)^l$ ...	3.533666	0.0191	+	2.8	3.2	1.0	1.1
$R(2,1)^u$ ...	3.538424	0.0182	+	-	-	-	-
$R(2,2)^u$ ...	3.542158	0.0094	+	-	-	-	-
$R(2,1)^l$ ...	3.615924	0.0044	-				
$R(2,2)^l$ ...	3.620473	0.0177	-				
$R(1,1)^u$ ...	3.668083	0.0158	+	11[c]	8.2[c]	2.5[d]	1.9[d]
$R(1,0)$ ...	3.668516	0.0259	+	11[c]	8.2[c]	1.2[d]	0.94[d]
$R(1,1)^l$ ...	3.715479	0.0141	+	5.1[e]	4.8[e]	2.3	2.2
$Q(3,3)$ ...	3.903967	0.0065	-				
$Q(2,2)$ ...	3.914406	0.0086	+	-	-	-	-
$Q(2,1)^u$ ...	3.916979	0.0043	+	-	-	-	-
$Q(1,1)$ ...	3.928625	0.0128	+	4.5	5.1	2.1	2.5
$Q(1,0)$ ...	3.953000	0.0254	+	5.2	5.0	1.3	1.2
$Q(2,1)^l$ ...	3.971073	0.0167	+	-	-	-	-
$Q(3,0)$ ...	3.985528	0.0249	+	-	-	-	-
$Q(3,1)^u$ ...	3.987028	0.0217	+	-	-	-	-
$P(1,1)$ ...	4.069524	0.0086	-				
$N_{\rm total}$ [10^{15} cm^{-2}]						4.6	4.4

[a] Lindsay & McCall (2001).

[b] J. K. G. Watson, private communication.

[c] Total equivalent width of $R(1,1)^u$ and $R(1,0)$.

[d] Column density of the each level is derived on the assumption that the populations in the ortho- (1, 0) and para- (1, 1) levels are divided into about 2 : 1, which is implied by $R(1,1)^l$, $Q(1,1)$ and $Q(1,0)$ transitions.

[e] Equivalent width of $R(1,1)^l$ is calculated from the Gaussian decomposition parameters. For other transitions W_λ are obtained by directly integrating the absorption features.

Table 2. Summary of observation.

Name	R.A. (J2000)	Dec. (J2000)	l [°]	b [°]	L	Exposure [s]	Grating[a] ECH	XDP	Standard Name	Spe.
GCS 3-2[b]...	17:46:14.8	-28:49:41	0.16	-0.06	2.7	120	8350	6100	HR 7528	B9.5IV
						240	4400	5200	HR 7528	B9.5IV
GC IRS 3[c]...	17:45:39.9	-29:00:24	-0.06	-0.04	5.3	360	8350	6100	HR 7924 (α Cyg)	A2Iae
						1440	4400	5200	HR 7924 (α Cyg)	A2Iae

[a] "ECH" and "XDP" denote the angle of echelle and cross-dispersing gratings in the instrumental unit.

[b] Coordinate and magnitude are from Nagata et al. (1990).

[c] Coordinate and magnitude are from Blum, Sellgren, & DePoy (1996).

Table 3. The velocity resolved components of $R(1,\,1)^l$, $Q(1,\,1)$ and $Q(1,\,0)$.

Name	$v_{\rm LSR}$ [km s^{-1}]	FWHM [km s^{-1}]	W_λ [10^{-5} μm]			$N_{\rm level}$ [10^{14} cm^{-2}]			$N_{\rm total}$ [10^{14} cm^{-2}]^a
			$R(1,\,1)^l$	$Q(1,\,1)$	$Q(1,\,0)$	$R(1,\,1)^l$	$Q(1,\,1)$	$Q(1,\,0)$	
GCS 3-2…	-165	15	0.15	-	-	0.7	-	-	1.3
	-107	50	1.8	2.0	1.2	8.3	9.4	2.9	16
	-51	38	1.9	1.7	2.1	8.6	7.9	5.1	17
	-2	31	1.2	1.5	1.7	5.6	7.0	4.1	11
GC IRS 3…	-140	22	0.64	-	0.30	2.9	-	0.51	5.6
	-56	15	0.27	-	0.46	1.2	-	1.1	2.4
	-23 [b]	116	3.7	-	3.0	17	-	7.2	32
	-5	12	0.50	-	0.73	2.3	-	1.7	4.3

[a] Based on the velocity independent conversion factor of $R(1,\,1)^l$ to total column density derived from Table 1.

[b] Pedestal component.

Fig. 1. Wavelength coverage of IRCS echelle mode in the 3 μm region. The entire L-band (2.84–4.18 μm) is covered by six standard settings (LA^-, LA_0, LA^+, LB^-, LB_0, LB^+; shown in green and blue rectangles) but 70% is covered by three settings. "ECH" and "XDP" denote the angles of the echelle and cross-disperser gratings. The grating angle can be seamlessly modified to best suite to individual project. The two settings we employed for the observation are shown by the bold-line enclosures. The positions of major H_3^+ lines are marked by sticks with the heights representing the relative intensities calculated with $T = 300$ K. The atmospheric transmission curve is overlaid to illustrate the region where the interference of the telluric atmospheric absorption is severe.

Fig. 2. The total detected H_3^+ absorption spectra toward GCS 3-2 (left column) and GC IRS 3 (right column). Kinematic components are indicated in the LSR velocity with dotted lines (See Figure 4). Note that the 3.668 μm line profile appears different from the others because it consists of a close doublet of $R(1, 0)$ and $R(1, 1)^u$ separated by $\Delta v = 35$ km s^{-1}. The feature is lined up with other absorption lines at $R(1, 0)$ 3.6685 μm. The model atmospheric transmission curves are shown to discriminate the genuine detections from the possible artifacts of the poor cancellation of the telluric absorption lines.

Fig. 3. Same with Figure 2, but for the negative detections. The periodic patterns seen at 3.97–3.98 μm are the instrumental fringes left unprocessed. Note that the dips at 3.534 μm in the bottom panels are $R(3, 3)^l$ positively detected.

Fig. 4. Gaussian decomposition of the kinematic components for GCS 3-2 (top) and GC IRS 3 (bottom). At least four components are found in ortho- $Q(1, 0)$ and para- $R(1, 1)^l$ and $Q(1, 1)$ H_3^+ absorption lines at common velocities. The residual of the fitting is shown at the bottom of the each panel. The decomposition parameters are summarized in Table 3.

Fig. 5. Comparison of the line profiles of H_3^+ at $R(1, 1)^l$ and $R(3, 3)^l$ along with those of other molecules and atom toward the same objects. GCS 3-2 is in the left, and GC IRS 3 in the right. The absorption spectra of the previous works are shown in arbitrary unit. The dotted lines represent the velocity components of the $R(1, 1)^l$ transition in the previous figure. Three velocity components in GC IRS 3 at -140 km s^{-1}, -60 km s^{-1}, and -0 km s^{-1} match well with CO $R(2)$, H_2CO and H I absorption, indicating the same absorbing clouds. The deep absorptions of CO and H_2CO at +50 km s^{-1} toward the Galactic center do not correspond to strong components in the H_3^+ spectrum, which might be accounted for by the compact structure of the absorbing cloud. Note the considerable difference in the line shape of $R(3, 3)^l$ from $R(1, 1)^l$ for both GCS 3-2 and GC IRS 3. The line profile of the $R(3, 3)^l$ in GC IRS 3 is more or less similar to that of CO absorption at 4.7 μm.

Fig. 6. A schematic of the number density variation of H_3^+ with respect to hydrogen along with that of major molecules and ions in the interstellar medium. The number density of H_3^+ is independent of $n(\mathrm{H})$ in contrast with the other molecules. We define "dense" and "diffuse" clouds by the form of carbon atoms. The form of carbon is critical since it defines the destruction mechanism of H_3^+, and hence the number density of the molecular ions.

Fig. 7. Rotational energy levels of H_3^+ in the ground state and in the ν_2 vibrationally excited state. H_3^+ has two vibrational modes of which only ν_2 is infrared active, and targeted in our observation. $G = |k - l_2|$ is used instead of K in the diagram, where l_2 is a vibrational angular momentum of ν_2. G is a better quantum number than K where $l_2 \neq 0$ (see McCall 2001 for detail). The letters u and l marked in the ν_2 state denote the levels of same G number but with different combinations of k and l_2. The major transitions of $\nu_2 \leftarrow 0$ that appear in the 3 to 4 μm regions are indicated by the vertical connecting arrows with labels. Note that for the ground vibrational state, $J = 2n$ and $G = 0$ levels are forbidden by the Pauli principle (shown in dotted bars). The lowest levels of ortho- $(J, G) = (1, 0)$ and para- $(J, G) = (1, 1)$ H_3^+ are marked with thick solid bars. The selection rule allows only radiative relaxation between two levels that satisfy $\Delta J = 0, \pm 1$ and $\Delta G = \pm 3$. The spontaneous transitions are indicated with connecting lines of energy levels in the ground state. The transition between $G = 2 \leftrightarrow 1$ can be understood to be $G = \pm 2 \leftrightarrow \mp 1$. The "+" and "−" signs in the ground state denote the parity of the energy levels. The parity rule, $+ \leftrightarrow -$, is automatically satisfied by $\Delta G = \pm 3$. The $(J, G) = (3, 3)$ and $(5, 5)$ are disconnected from any lower levels by the selection rule, making the two levels metastable (Pan & Oka 1986). The (4, 4) level can be relaxed to (3, 1), but has a long lifetime.

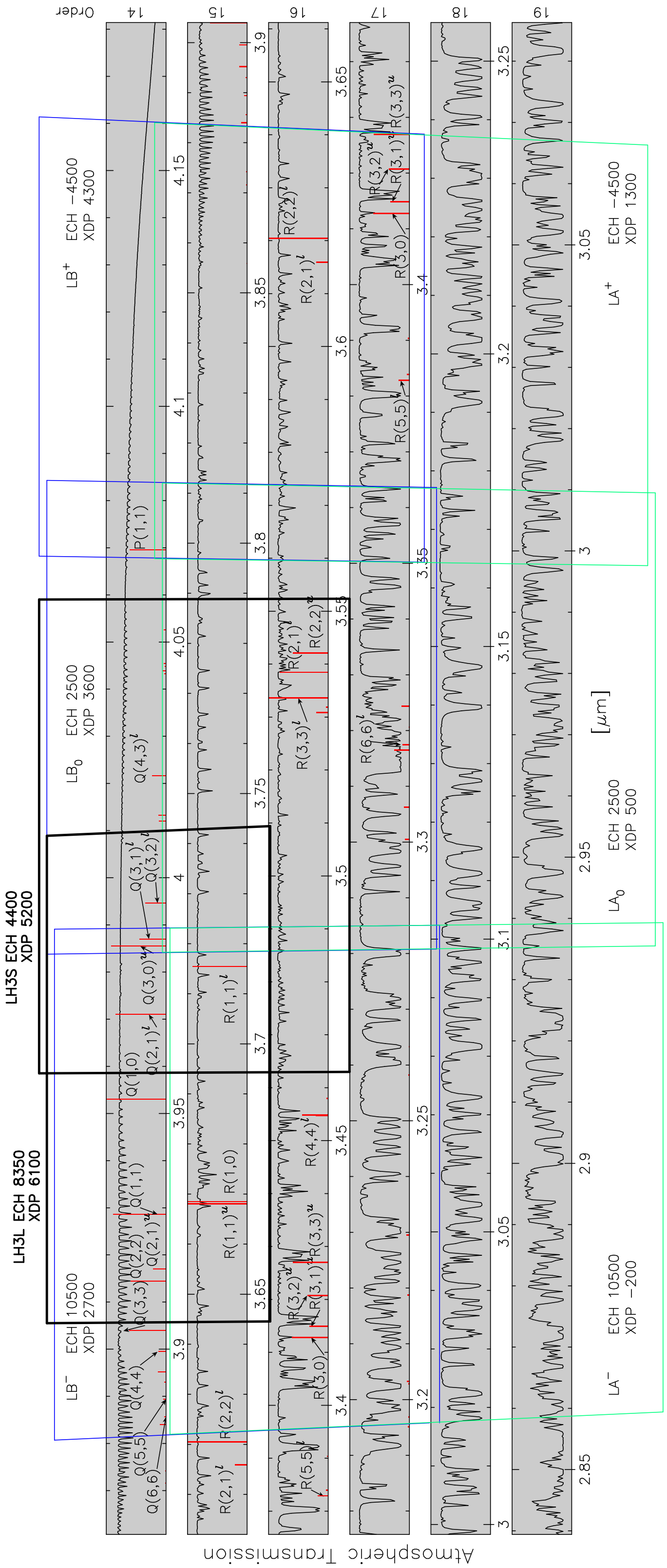

LH3L ECH 8350
XDP 6100
LH3S ECH 4400
XDP 5200
LB⁻ ECH 10500
XDP 2700
LB₀ ECH 2500
XDP 3600
LB⁺ ECH −4500
XDP 4300
LA⁻ ECH 10500
XDP −200
LA₀ ECH 2500
XDP 500
LA⁺ ECH −4500
XDP 1300
Order
Atmospheric Transmission
[μm]

Fig. 1.

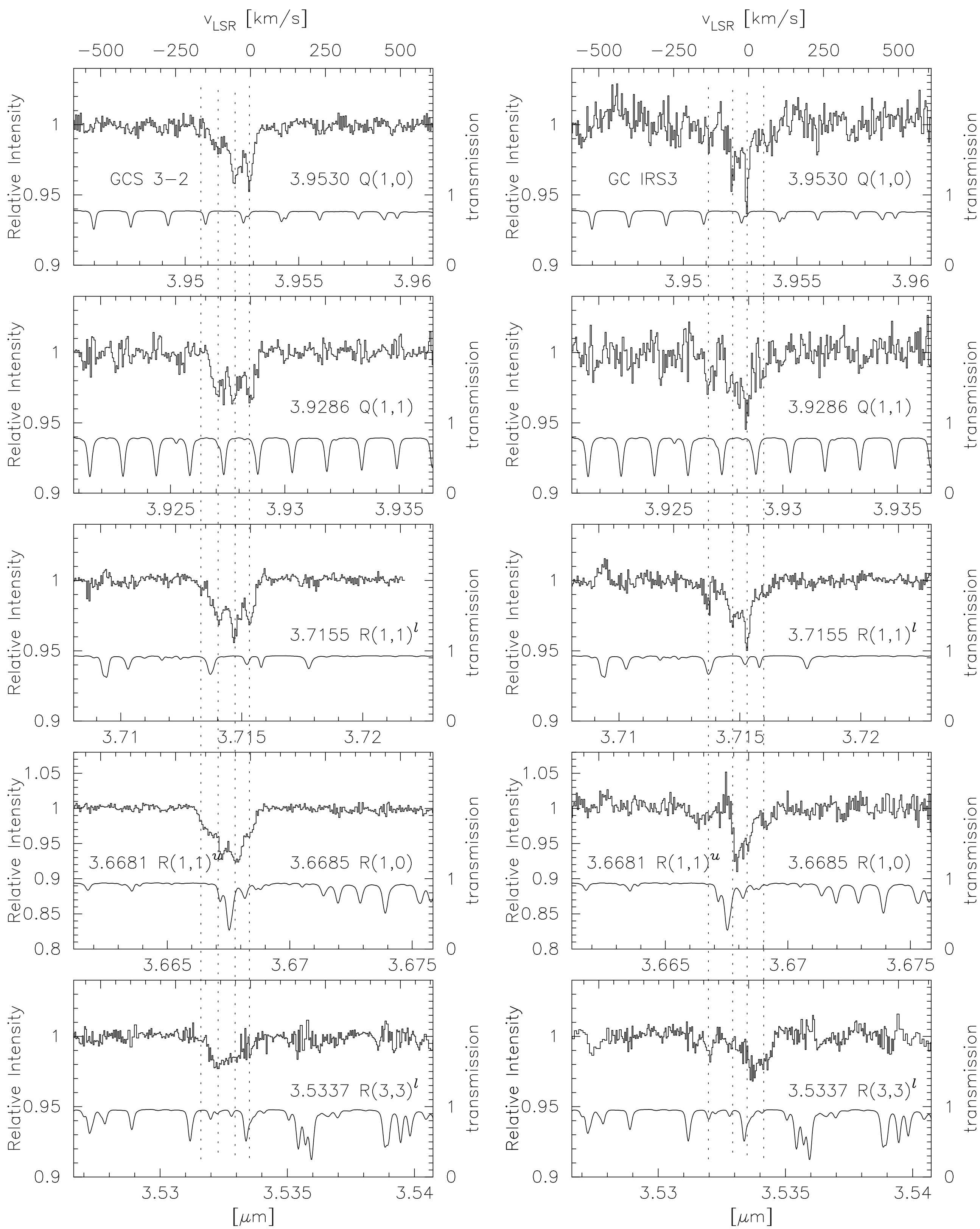

v_LSR [km/s]
−500 −250 0 250 500
Relative Intensity
transmission
GCS 3−2
GC IRS3
3.9530 Q(1,0)
3.9286 Q(1,1)
3.7155 R(1,1)^l
3.6681 R(1,1)^u
3.6685 R(1,0)
3.5337 R(3,3)^l
[μm]

Fig. 2.

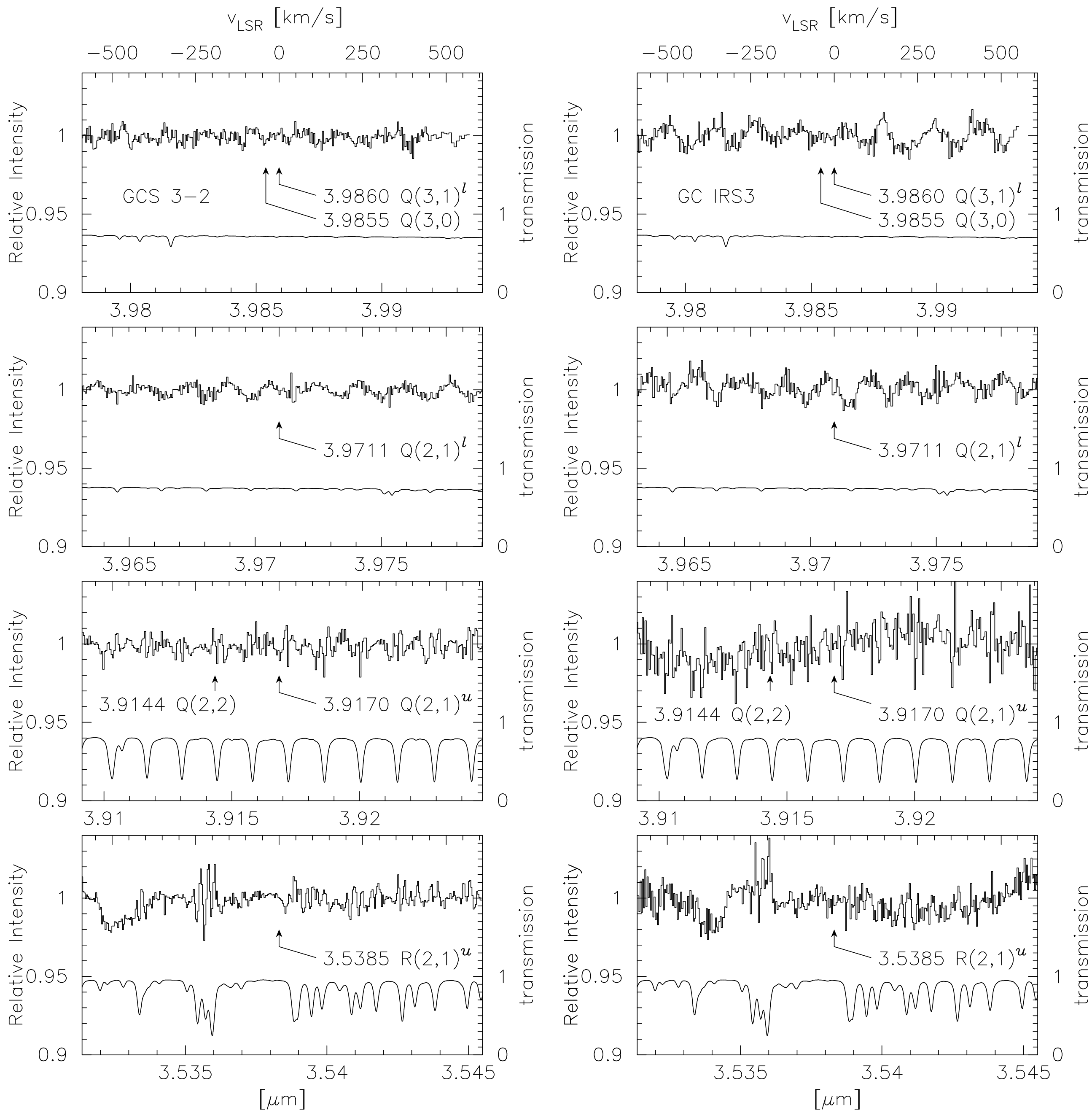

v_LSR [km/s]
−500 −250 0 250 500
Relative Intensity
transmission
GCS 3−2
GC IRS3
3.9860 Q(3,1)^l
3.9855 Q(3,0)
3.9711 Q(2,1)^l
3.9144 Q(2,2)
3.9170 Q(2,1)^u
3.5385 R(2,1)^u
[μm]

Fig. 3.

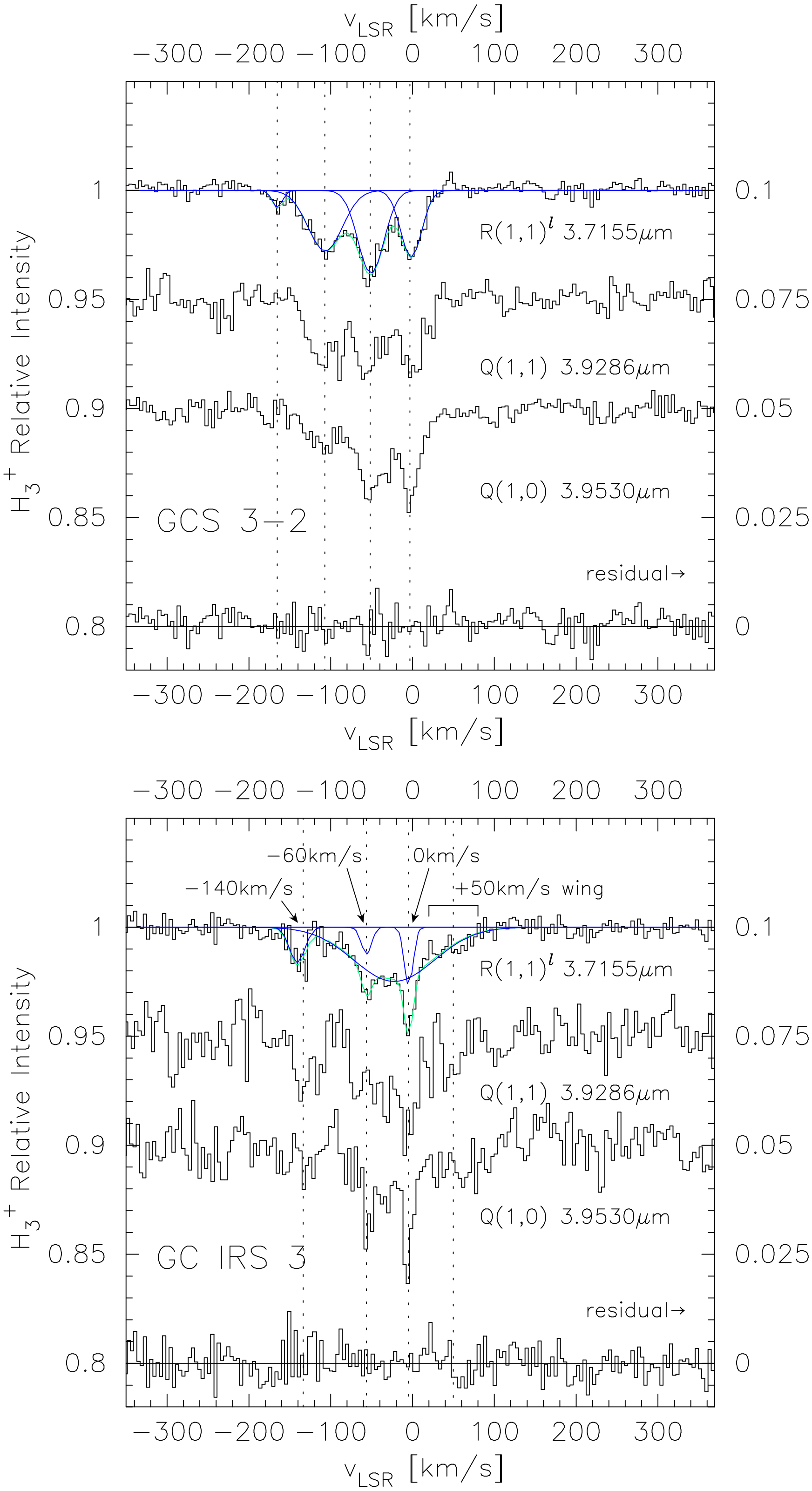

v_LSR [km/s]
−300 −200 −100 0 100 200 300
H3+ Relative Intensity
1
0.95
0.9
0.85
0.8
0.1
0.075
0.05
0.025
0
R(1,1)^l 3.7155μm
Q(1,1) 3.9286μm
Q(1,0) 3.9530μm
GCS 3−2
residual→
−60km/s
0km/s
−140km/s
+50km/s wing
GC IRS 3

Fig. 4.

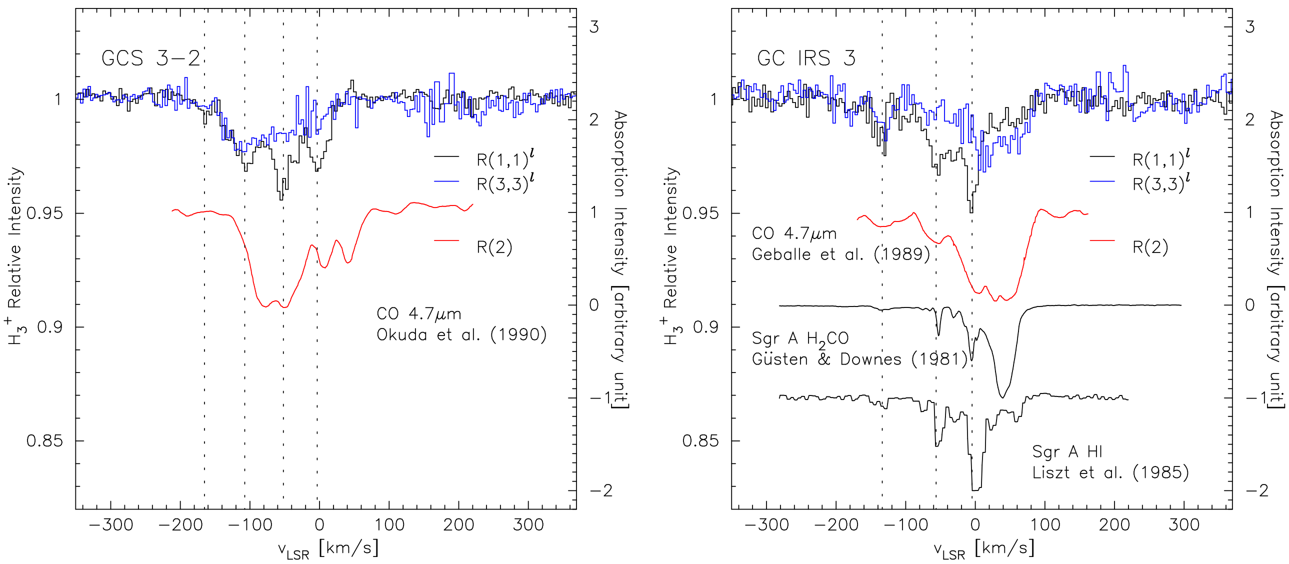

GCS 3−2
R(1,1)^l
R(3,3)^l
R(2)
CO 4.7μm
Okuda et al. (1990)
GC IRS 3
CO 4.7μm
Geballe et al. (1989)
Sgr A H2CO
Güsten & Downes (1981)
Sgr A HI
Liszt et al. (1985)
H3+ Relative Intensity
Absorption Intensity [arbitrary unit]
vLSR [km/s]

Fig. 5.

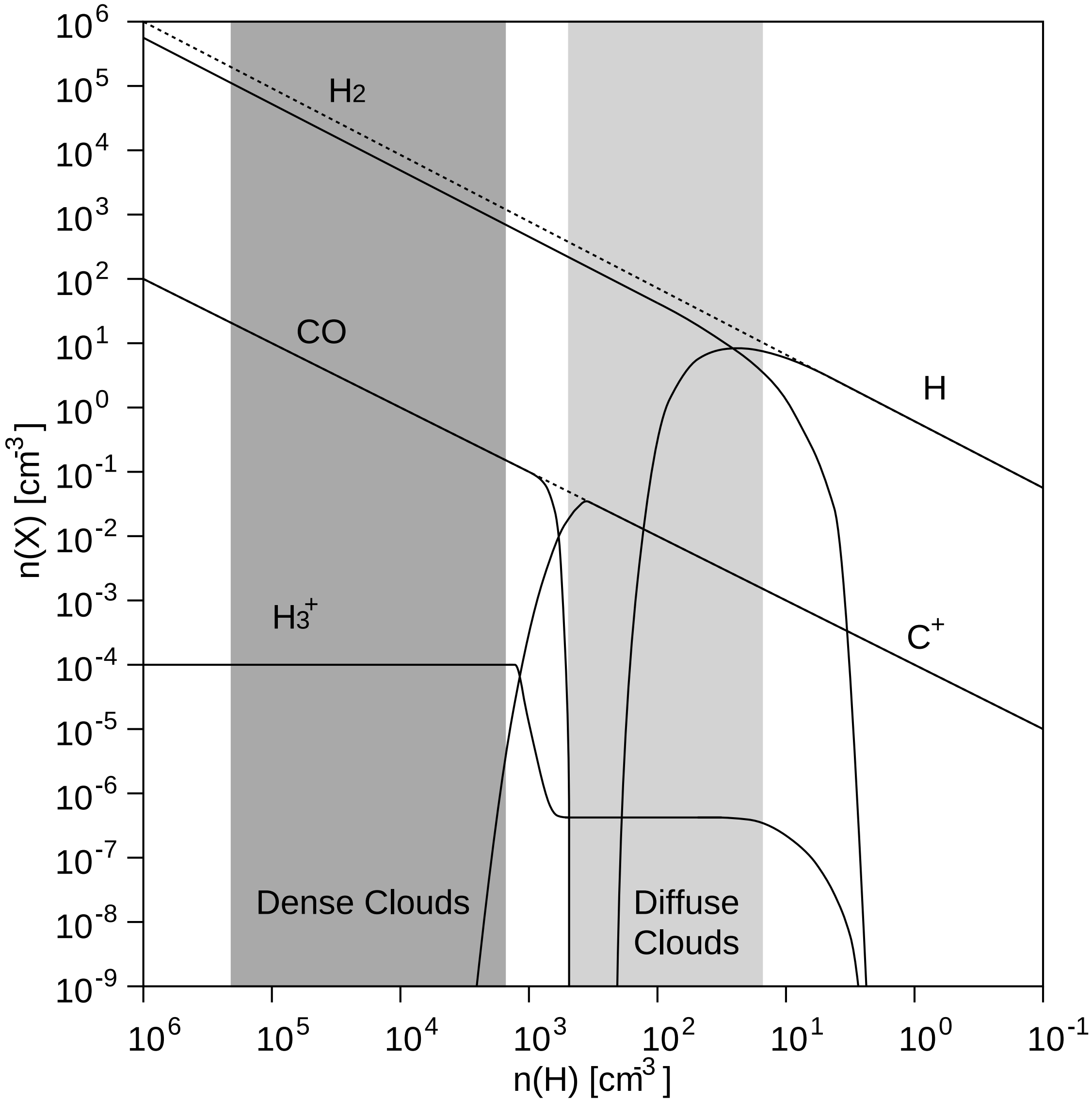

10^6
10^5
10^4
10^3
10^2
10^1
10^0
10^{-1}
10^{-2}
10^{-3}
10^{-4}
10^{-5}
10^{-6}
10^{-7}
10^{-8}
10^{-9}
n(X) [cm^{-3}]
H_2
CO
H_3^+
H
C^+
Dense Clouds
Diffuse
Clouds
10^6
10^5
10^4
10^3
10^2
10^1
10^0
10^{-1}
n(H) [cm^{-3}]

Fig. 6.

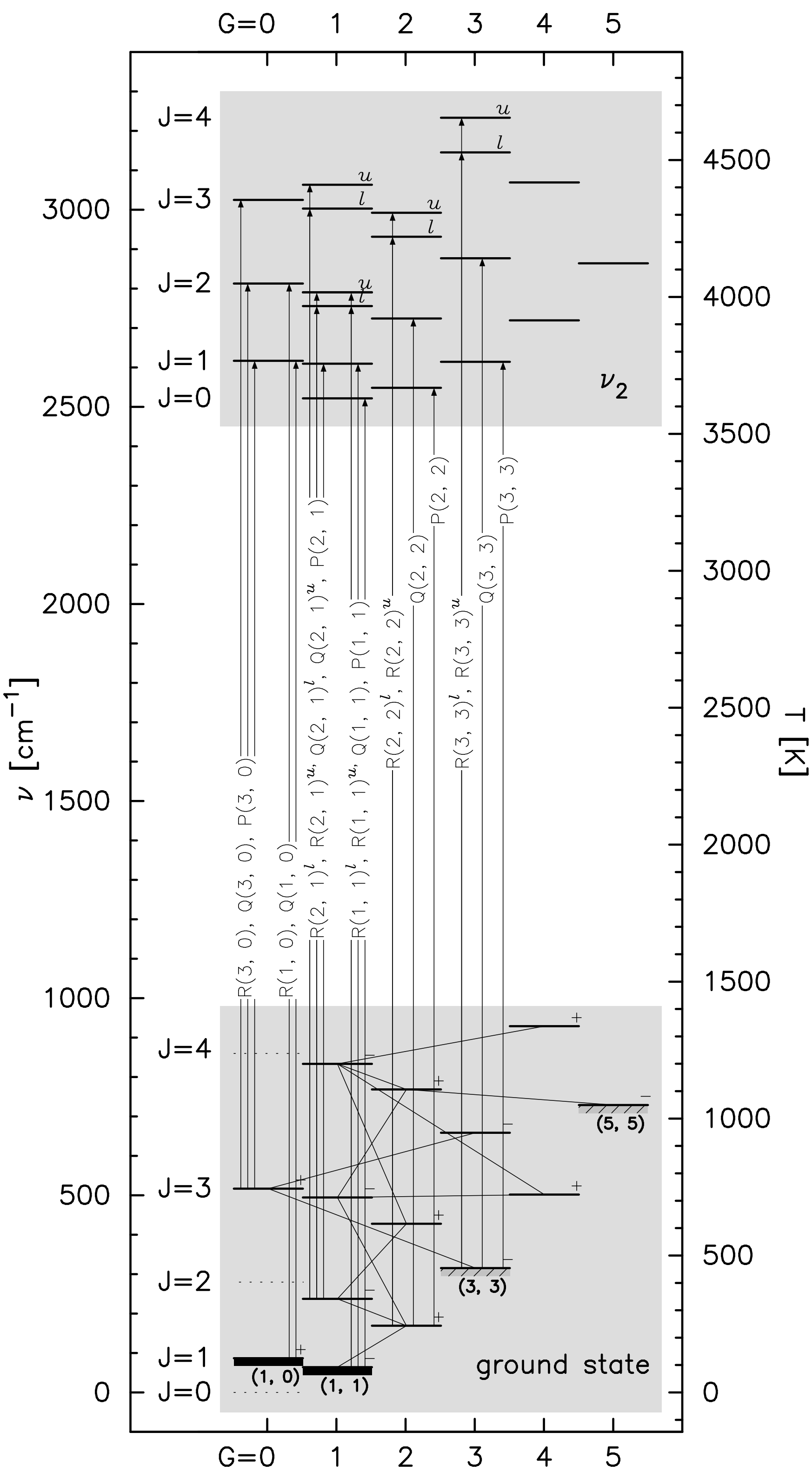
G=0
1
2
3
4
5
J=4
J=3
J=2
J=1
J=0
u
l
ν_2
R(3, 0), Q(3, 0), P(3, 0)
R(1, 0), Q(1, 0)
R(2, 1)^l, R(2, 1)^u, Q(2, 1)^l, Q(2, 1)^u, P(2, 1)
R(1, 1)^l, R(1, 1)^u, Q(1, 1), P(1, 1)
R(2, 2)^l, R(2, 2)^u
Q(2, 2)
P(2, 2)
R(3, 3)^l, R(3, 3)^u
Q(3, 3)
P(3, 3)
(1, 0)
(1, 1)
(3, 3)
(5, 5)
ground state
ν [cm^{-1}]
T [K]

Fig. 7.